PNAS RESEARCH ARTICLE | NEUROSCIENCE OPEN ACCESS

Adeno-associated viruses for efficient gene expression in the axolotl nervous system

Katharina Lust[a,1] and Elly M. Tanaka[a,1]

Contributed by Elly M. Tanaka; received October 16, 2024; accepted January 27, 2025; reviewed by Justus M. Kebschull, Lora Sweeney, and Maria Antonietta Tosches

Axolotls are amphibian models for studying nervous system evolution, development, and regeneration. Tools to visualize and manipulate cells of the axolotl nervous system with high-efficiency, spatial and temporal precision are therefore greatly required. Recombinant adeno-associated viruses (AAVs) are frequently used for in vivo gene transfer of the nervous system but virus-mediated gene delivery to the axolotl nervous system has not yet been described. Here, we demonstrate the use of AAVs for efficient gene transfer within the axolotl brain, the spinal cord, and the retina. We show that serotypes AAV8, AAV9, and AAVPHP.eB are suitable viral vectors to infect both excitatory and inhibitory neuronal populations of the axolotl brain. We further use AAV9 to trace retrograde and anterograde projections between the retina and the brain and identify a cell population projecting from the brain to the retina. Together, our work establishes AAVs as a powerful tool to interrogate neuronal organization in the axolotl.

axolotl | adeno-associated viruses | viral circuit tracing | salamander

Significance

Amphibians occupy a central position in the phylogeny of tetrapods and serve as a valuable model system for integrating studies of behavior with the cellular and circuit-level biology of the nervous system. Notably, the salamander *Ambystoma mexicanum* (axolotl) is an emerging genetic model for investigating neural circuit regeneration. However, research on amphibian nervous systems has been hindered by the absence of viral tools for gene delivery into postmitotic neurons. In this study, we address this gap by introducing viral transduction techniques for the axolotl nervous system through a comprehensive characterization of Adeno-associated viruses for successful gene delivery, enabling projection mapping in the axolotl brain, spinal cord, and retina.

Salamanders such as axolotls (*Ambystoma mexicanum*) can regenerate injuries to the central and peripheral nervous system making them an ideal model to study formation and regeneration of neural circuits. The regeneration of neural circuits in salamanders has been demonstrated to occur across multiple regions of the central nervous system. For instance, retinotectal projections can be reestablished following the removal of the optic tectum in adult newts (1). Similarly, in axolotls, long-distance projections, and input connections from and to the regenerated dorsal telencephalon can recover to varying extents (2, 3). These findings have been primarily obtained using classical tracers, calcium imaging in ex vivo brain slices, and diffusion tensor imaging; however, these techniques are limited in both resolution and dynamic range (3–6). To map the dynamics of neural circuit regeneration, to understand their capacity for functional recovery, and to manipulate their function effectively, there is a critical need for advanced tools that enable efficient labeling and manipulation of cells within the nervous system.

Transgenesis (7), electroporation, (8) and virus-mediated gene delivery (9) are established methodologies for introducing genes into salamander cells. Several virus-mediated gene delivery tools including pseudotyped Moloney murine leukemia virus (10), vaccinia virus (11), foamy virus (12), and pseudotyped baculovirus (9) were shown to be functional and efficient for transduction of cells in the axolotl limb where they infect muscle, cartilage, dermis, fibroblasts, and Schwann cells (9, 12). Virus-mediated gene delivery to axolotl nervous system tissue has not been achieved so far. Neuron-targeted gene delivery in the central and peripheral nervous system is challenging because neurons are postmitotic. For that purpose, Adeno-associated viruses (AAVs) and lentiviruses are commonly used viral vectors in neuroscience (13, 14). While lentivirus has been utilized in axolotls, the observed expression levels are notably low. Especially in vivo hardly any expression of lentivirus-mediated transgenesis has been observed (12). Use of AAVs has so far not been described in the axolotl.

AAVs belong to the genus *Dependoparvovirus*, which is part of the *Parvoviridae* family and are characterized by their small size, nonenveloped structure, and replication-defective nature and their genome consists of a linear single-stranded DNA of approximately 4.7 kilobases in length (15). AAVs are particularly attractive candidate vectors because in contrast to most viruses, they possess no intrinsic pathogenicity, low immunogenicity, long transgene expression, and a wide-ranging tropism (15). The utilization of AAV-mediated delivery for introducing genetic material into specific populations of the nervous system represents a valuable strategy for investigating both anatomy and circuit function. AAVs possess two key components that can be engineered: the capsid (the outer protein shell) and the encapsulated genome (cargo) (16). Modifying the capsid allows for the enhancement of cell type or tissue specificity (tropism), while adjustments to the cargo can regulate

Author affiliations: [a]Institute of Molecular Biotechnology of the Austrian Academy of Sciences (IMBA), Vienna Biocenter (VBC), Vienna 1030, Austria

Author contributions: K.L. and E.M.T. designed research; K.L. performed research; K.L. analyzed data; and K.L. and E.M.T. wrote the paper.

Reviewers: J.M.K., Johns Hopkins University; L.S., Institute of Science and Technology Austria; and M.A.T., Columbia University.

The authors declare no competing interest.

[1]To whom correspondence may be addressed. Email: katharina.lust@imba.oeaw.ac.at or elly.tanaka@imba.oeaw.ac.at.

This article contains supporting information online at https://www.pnas.org/lookup/suppl/doi:10.1073/pnas.2421373122/-/DCSupplemental.

Published March 5, 2025.

transgene expression (17). Advances in capsid engineering have led to the development of several AAV variants with specialized properties, such as improved transduction efficiency in the central nervous system (18) and specificity for certain cell types (17). By entering either at somata or axon terminals, anterograde and retrograde projections can be assessed allowing to map input and output projections of defined regions (19). Additionally, AAV-driven gene expression can be stable and sustained for extended periods without causing significant adverse effects on neuronal health. Combining AAVs with advanced gene regulatory elements, reporters for calcium imaging, optogenetic or chemogenetic probes, and effector genes makes them valuable for the visualization and manipulation of neural circuits (20).

AAV vectors, widely employed in rodents and other mammals (21), have recently found application in avian species such as pigeon (22) and songbirds (23, 24), in the reptile *Pogona vitticeps* (25) as well as in the salamander *Pleurodeles waltl* and the frog *Xenopus laevis* (26). In contrast, AAVs fail to infect neurons in zebrafish (27). Several studies have conducted comparative evaluations of AAV serotypes, and it has been demonstrated that the tropism of AAVs for distinct organs and tissues varies depending on their serotype (17, 26). Importantly, the transduction efficacy of a serotype is not simply predictable from one model system to another.

Here, we present a set of AAV serotypes with high transfection efficiency for the axolotl brain and retina. In short, we tested seven AAV serotypes for their infection and expression efficiency and found that AAV8, AAV9, AAVRG, and AAVPHP.eB are most suited to label neurons of the brain. Moreover, AAV8, AAV9, and AAVPHP.eB are also suited to label cells of the spinal cord and map neuronal projections. We also investigate the use of AAVs to label input and output projections of the retina through anterograde and retrograde tracing. We define AAV9 as the most suitable AAV to label retinal cells and use it to trace projections from the retina to various brain regions. Additionally, we identify a retinopetal cell population in the axolotl which projects from the hypothalamus to the retina.

Results

Comparative Transduction Analysis of AAV Serotypes in the Axolotl Brain. AAV serotypes have been determined to infect different organs in mammalian model systems with various efficiencies (17). As the use of AAVs has not yet been described in the axolotl, we first explored which serotypes can efficiently infect cells of their central nervous system. For this, we tested seven commonly used AAV serotypes: AAV1, AAV2, AAV5, AAV8, AAV9, AAVRG, and AAVPHP.eB. To distinguish lack of transduction from lack of expression we used the same transgene CAG:GFP-WPRE-SV40PolyA in each virus. We injected the optic tectum parenchyma of ten animals of a size of 3 cm (nose to tail) with each serotype and observed them under a fluorescent widefield microscope for a period of 4 wk (Fig. 1*A* and *SI Appendix*, Fig. S1). Four weeks after injection the green fluorescence was visible (*SI Appendix*, Fig. S1). Notably, AAV8-CAG:GFP, AAV9-CAG:GFP, and AAVPHP.eB-CAG:GFP displayed strong expression in the brain when observed in live animals (*SI Appendix,* Fig. S1). In contrast, expression of GFP was barely detectable in live animals transfected with AAV2-CAG:GFP (one out of 10 animals positive, *SI Appendix,* Fig. S1 *A* and *C*). At 4 wk postinjection, we harvested the brains and performed wholemount immunostaining for GFP (Fig. 1 *B*–*H*). We aimed to determine whether brains with low expression (live animals, at the stereomicroscope) were devoid of GFP-expressing neurons (i.e., lack of infection) or whether the expression of GFP was low and could be amplified with immunostaining. We found abundant GFP-expressing neurons in the optic tectum transduced with each serotype except AAV2 (six neurons in one out of 10 brains, Fig. 1 *C* and *I*). We then quantified the density of GFP-positive neurons in a defined volume of 200 × 200 × 80 μm^3, normalized to the respective viral titers and found that AAV8-CAG:GFP, AAV9-CAG:GFP, and AAVPHP.eB-CAG:GFP showed the highest efficiency to label cells around the injection site (Fig. 1*I*). Especially AAVPHP.eB-CAG:GFP showed a high density of labeled cells which reached almost twice as much as AAV8-CAG:GFP and AAV9-CAG:GFP. We additionally used cryosections and quantified the efficiency of infection over a region of 250 × 250 μm^2 for AAV8-CAG:GFP, AAV9-CAG:GFP, and AAVPHP.eB-CAG:GFP, normalized to the respective viral titers (Fig. 1*J*). This showed that AAVPHP.eB-CAG:GFP reached an efficiency of 7.7% of cells while AAV8-CAG:GFP, AAV9-CAG:GFP infect 4.9% of cells and 5.2% of cells respectively (Fig. 1*J*).

We have previously used axolotls of a larger size (10 cm nose to tail) for studying brain regeneration (3). While these stages are not yet sexually mature, they show a full spectrum of swimming and walking behaviors and are largely comparable in brain size and stem cell proliferation to sexually mature animals (2). We therefore also tested the feasibility and efficiency of AAV-mediated transduction in these animals. We decided to use only the AAVs which had worked best in small axolotls and therefore injected AAV8-CAG:GFP, AAV9-CAG:tdTomato, AAVRG-CAG:tdTomato as well as AAVPHP.eB-CAG:GFP into one hemisphere of the dorsal telencephalon of three animals each (*SI Appendix,* Fig. S2). Four weeks after injection, we fixed the brains and analyzed by wholemount immunostaining for transgene expression. We found that all four tested serotypes infected cells in 10 cm axolotl brains (*SI Appendix,* Fig. S2 *B*–*G*). Taken together, all tested AAV serotypes except AAV2 can be used to deliver genes into brains of larval and juvenile axolotls.

AAV8, AAV9, and PHP.eB Preferentially Label Neuronal Cells. The two most abundant cell types in the axolotl brain are neurons and ependymoglia (3). The CAG promoter can drive transgene expression in all cell types and has been used previously in axolotl for ubiquitous transgene expression (28). We therefore analyzed the extent to which GFP-expressing cells were colocalized with either a glial or a neuronal marker in sections of brains infected with AAV8-CAG:GFP, AAV9-CAG:GFP, and AAVPHP.eB-CAG:GFP. We performed combined immunofluorescence stainings on cryosections against GFP to visualize transduced cells and against glial fibrillary acidic protein (GFAP) to visualize ependymoglia. We found that AAV8-CAG:GFP (Fig. 2 *A* and *D*), AAV9-CAG:GFP (Fig. 2 *B* and *D*), and AAVPHP.eB-CAG:GFP (Fig. 2 *C* and *D*) showed significantly higher transgene expression in neurons than in ependymoglia cells, with a maximum of four ependymoglia cells labeled per 18 µm section (Fig. 2 *A*–*D*). Thus, even though not specifically targeted to express in neurons AAV8-CAG:GFP, AAV9-CAG:GFP, and AAVPHP.eB-CAG:GFP show preferential neuronal expression after 1 mo of AAV delivery. The expression of transgenes in neurons observed 1 mo after AAV injection could be attributed to the transduction of ependymoglia, which generate new neurons during postembryonic growth. Alternatively, AAVs injected into the ventricle might directly transduce neurons that were already postmitotic at the time of injection. To directly determine whether AAVs can transduce differentiated neurons, we employed in situ hybridization chain reaction (HCR) (29) using probes specific to regions of the viral genome and viral mRNA. Three days postinjection, viral DNA/RNA was detected in both radial glia within the ventricular zone and in neurons located in

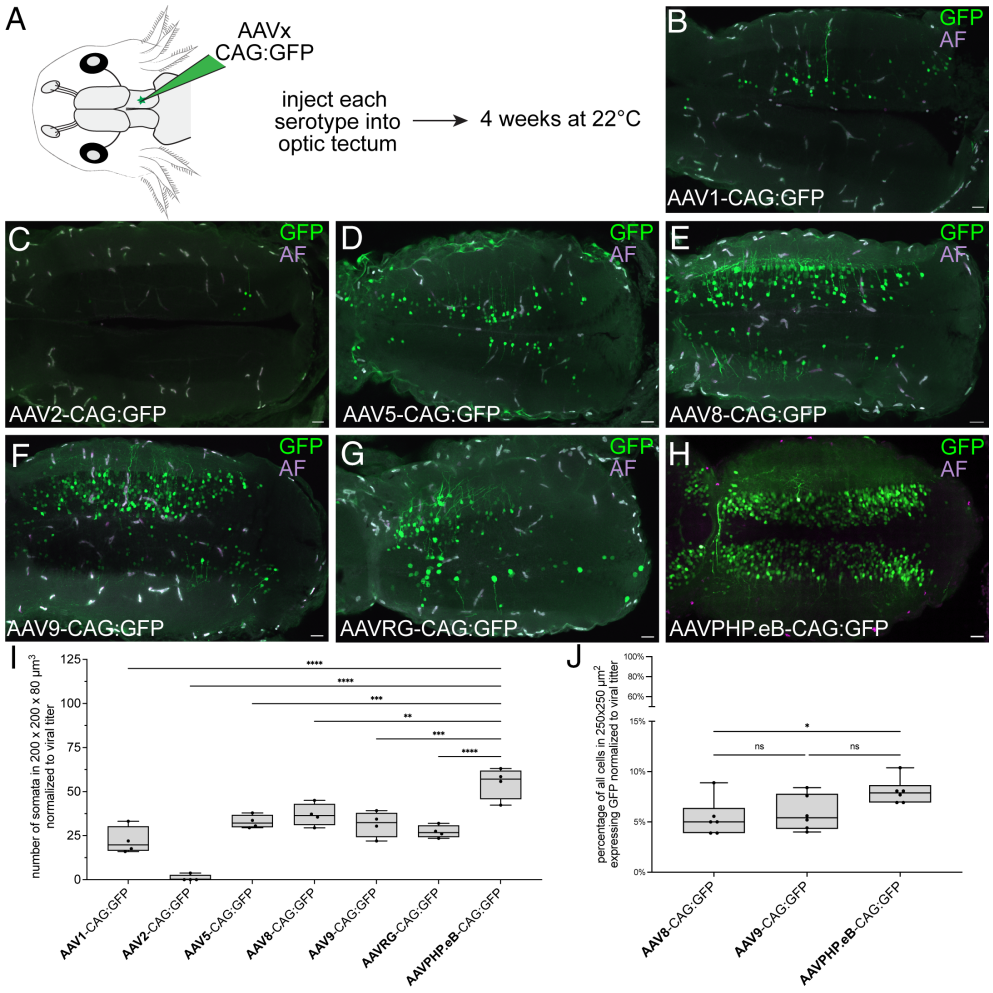

Fig. 1. AAV-mediated cell transduction in the larval axolotl brain. (*A*) Schematic of experimental paradigm for AAV serotype efficiency test. Each serotype was injected into the right optic tectum parenchyma of larval (3 cm nose to tail) animals which were housed at 22 degrees for 4 wk until the analysis. (*B–H*) Immunofluorescence for GFP (green) and autofluorescence (AF, magenta-white) on wholemount, cleared brains at 4 wk after AAV injection. (Scale bars, 100 µm.) (n = 10 axolotl for each serotype). (*I*) Quantification of GFP-positive somata per 200 × 200 × 80 μm^3 normalized to the viral titer. Boxplot indicates "minimum," first quartile, median, third quartile, and "maximum." Statistical significance is calculated using one-way ANOVA followed by Tukey's multiple comparison *P* values are $^{**}P = 0.0068$, $^{***}P = 0.0004$, $^{****}P < 0.0001$ (n = 4 axolotl for each serotype. The injection site was selected to be the center of the optic tectum. A region with strong expression in the center was selected and the volume around was quantified). (*J*) Quantification of the percentage of all cells expressing GFP per 250 × 250 μm^2 in sections of AAV8-CAG:GFP, AAV9-CAG:GFP, and AAVPHP.eB-CAG:GFP transduced brains normalized to the viral titer. Boxplot indicates "minimum," first quartile, median, third quartile, and "maximum." Statistical significance is calculated using one-way ANOVA followed by Tukey's multiple comparison *P* values are AAV8-CAG:GFP vs. AAV9-CAG:GFP ns = 0.8621, AAV8-CAG:GFP vs. AAVPHP.eB-CAG:GFP * = 0.0355 and AAV9-CAG:GFP vs. AAVPHP.eB-CAG:GFP ns = 0.0940 (n = 3 axolotl, quantification of two sections per animal, 250 × 250 μm^2 was selected as the DAPI positive the region including ependymoglia and neuronal layers).

the neuronal layers ranging from the cells closest to the ventricle until the furthest. The neurons harboring viral DNA were likely already differentiated at the time of injection based on previous estimations of neurogenesis rates and as neurons do not show migration in the axolotl midbrain (30).

Next, we investigated the ability of AAV8-CAG:GFP, AAV9-CAG:GFP, and AAVPHP.eB-CAG:GFP to transduce excitatory versus inhibitory neurons of the axolotl brain (*SI Appendix,* Fig. S3 *A–C*). To facilitate identification of excitatory and inhibitory neurons we used HCR in situ for Solute carrier family 17 member 7 *(Slc17a7)* and *Glutamate decarboxylase 2 (Gad2).* We found both GFP, *Slc17a7*-double positive and GFP, *Gad2*-double positive neurons in each infection (*SI Appendix,* Fig. S3 *A–C*), indicating that AAV8-CAG:GFP, AAV9-CAG:GFP, and AAVPHP.eB-CAG:GFP can infect and drive transgene expression in both excitatory and inhibitory neurons in the axolotl brain. Importantly, these results are qualitative and do not determine potential differences in infection rates.

Commonly employed promoters for gene expression in mammalian systems include the human synapsin (hSyn) promoter, which is neuron-specific, and the calcium/calmodulin-dependent protein kinase II alpha (CamKIIa) promoter, which can target excitatory neurons and inhibitory neurons (31). To evaluate the efficacy of these promoters in the axolotl, we conducted optic tectum injections using AAV8 vectors encoding GFP under the control of the hSyn (AAV8-hSyn:GFP-hGHpolyA) or CamKIIa (AAV8-CamKIIa:GFP-hGHpolyA) promoters, with AAV8-CAG:GFP serving as a positive control. One month postinjection, the brains were harvested and subjected to whole-mount immunostaining for GFP to account for potentially low expression due to the weaker hGHpolyA in the Syn and CamKIIa vectors. While all AAV8-CAG:GFP injected brains showed expression, no GFP-positive cells were observed in the brains injected with AAV8-hSyn:GFP or AAV8-CamKIIa:GFP (*SI Appendix,* Fig. S3*D*), suggesting that these promoters are ineffective in driving gene expression in the axolotl system.

AAV-Mediated Transduction of the Axolotl Spinal Cord. Axolotls are frequently utilized as a model organism to study spinal cord regeneration (32), where AAVs can be valuable tools for tracing

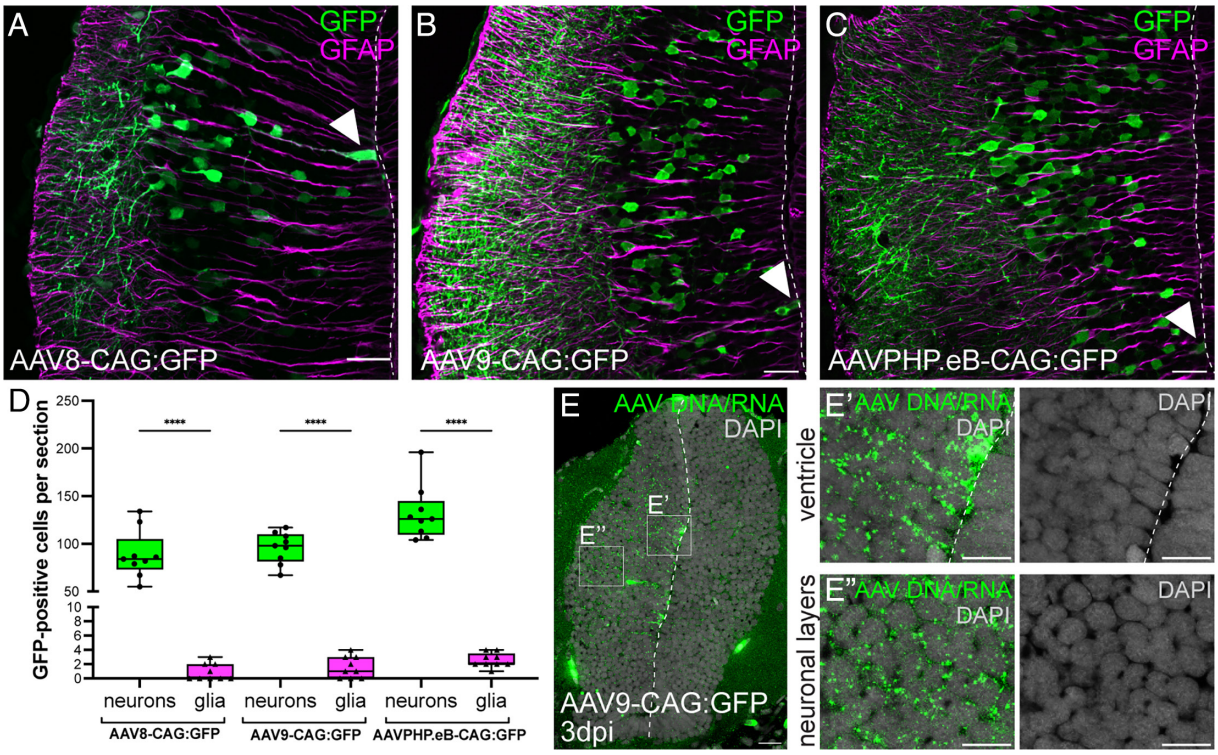

Fig. 2. AAV8, AAV9, and PHP.eB preferentially label neuronal cells. (*A–C*) Confocal image of expression of AAV8-CAG:GFP, AAV9-CAG:GFP, and AAVPHP.eB-CAG:GFP in neurons versus ependymoglia. Each serotype was injected into the right optic tectum parenchyma of larval (3 cm nose to tail) animals which were housed at 22 degrees for 4 wk until the analysis. Colabeling of cells was revealed by immunostaining against GFP (green) and GFAP (magenta). White arrowheads indicate labeled ependymoglia cells. White dashed lines indicate the ventricle. (Scale bars, 50 μm.) (*D*) Quantification of GFP-positive neurons versus glia in AAV8-CAG:GFP, AAV9-CAG:GFP, and AAVPHP.eB-CAG:GFP transduced brains. Boxplot indicates "minimum," first quartile, median, third quartile, and "maximum." Statistical significance is calculated using the unpaired *t* test, $^{****}P < 0.0001$. (n = 3 axolotl, quantification of three sections per animal). (*E*) Confocal image of optic tectum at 3 d after AAV9-CAG:GFP injection, showing the presence of viral DNA/RNA (green) in ependymoglia at the ventricle and neurons in the neuronal layers. Boxes indicate magnified regions. White dashed lines indicate the ventricle. (Scale bar in E is 50 μm, Scale bars in E′ and E″ are 25 μm.)

the reestablishment of neuronal projection patterns. To evaluate the potential of AAVs for transduction in the axolotl spinal cord, we analyzed the transduction efficiency of AAV serotypes that were previously shown to effectively transduce the brain. We injected AAV8-CAG:GFP (*SI Appendix*, Fig. S4), AAV9-CAG:GFP (Fig. 3 *B* and *C*), and AAVPHP.eB-CAG:GFP (Fig. 3 *D* and *E*) into the cervical spinal cord region of axolotls (5 cm in length from nose to tail) (Fig. 3*A*). At 1 mo postinjection, tissues were harvested from the hindbrain, extending through the cervical spinal cord to the lumbar region, and subjected to whole-mount immunostaining for GFP and the motor neuron marker choline acetyltransferase (ChAT). Both the injected region (cervical spinal cord) and a more posterior region (thoracic spinal cord) were imaged to assess the presence of transduced cells and projection patterns. We observed abundant GFP-positive cells within the spinal cords transduced by all tested AAV serotypes (Fig. 3 *B–E* and *SI Appendix*, Fig. S3 *B* and *C*). In the spinal cords injected with AAV9-CAG:GFP and AAVPHP.eB-CAG:GFP, we identified labeled motor neurons through costaining with ChAT (Fig. 3 *F* and *F′* and *SI Appendix*, Fig. S4 *D–D″*). In more posterior regions, specifically within the thoracic spinal cord, numerous GFP-positive projections were detected. Additionally, AAV9-CAG:GFP enabled the labeling of the Mauthner cell in the hindbrain, distinguishable by its location and large cell body (Fig. 3*H*). These results demonstrate that AAV8-CAG:GFP, AAV9-CAG:GFP, and AAVPHP.eB-CAG:GFP are capable of efficiently transducing cells within the axolotl spinal cord.

Immune Cell Infiltration and Glial Activation after AAVPHP.eB-Mediated Neuronal Transduction. Inflammation and glial cell activation associated with AAV administration have been observed after AAV delivery to the brain and retina and depend on many factors, including the AAV serotype, AAV dose, and AAV quality and nature of the transgene (33, 34). To investigate whether inflammation and glial activation occurs after transduction of axolotl neurons we infected brains with either AAV8-CAG-GFP:GFP, AAV9-CAG:GFP:GFP, AAVRG-CAG:GFP:GFP, and AAVPHP.eB-CAG:GFP and waited for 4 wk to reach high expression. We also performed a Sham injection as a control. We then performed stainings against GFP, ionized calcium binding adaptor molecule 1 (Iba1), and GFAP on cryosections (Fig. 4). Iba1 is a microglia/macrophage-specific calcium-binding protein which can be used to determine their activation and infiltration (35) while GFAP, a marker for ependymoglia cells in the axolotl brain (3), is used to determine astrocyte activation after stress or injury to the brain (36). We found that brains infected with AAV8-CAG:GFP (Fig. 4 *B* and *F*), AAV9-CAG:GFP (Fig. 4 *C* and *F*), and AAVRG-CAG:GFP (Fig. 4 *D* and *F*) only display low numbers of Iba1-positive cells (on average 4 to 9 Iba1-positive cells per 18 μm section) which are not significantly increased compared to Sham injected brains (Fig. 4 *A* and *F*) (on average 8 Iba1-positive cells per 18 μm section). In contrast to that, brains transduced with AAVPHP.eB-CAG:GFP showed strongly increased infiltration of Iba1-positive cells when compared to all other brains (on average 38 Iba1-positive cells per 18 μm section, Fig. 4 *E* and *F*). However, reactive ependymoglia, detectable by increased GFAP levels (37) were not found at 4 wk after any AAV transduction (*SI Appendix*, Fig. S5). Together, this shows that only AAVPHP.eB-CAG:GFP induces a strong increase of immune cells, while AAV8-CAG-GFP:GFP, AAV9-CAG:GFP:GFP, AAVRG-CAG:GFP:GFP show immune cell levels comparable to sham.

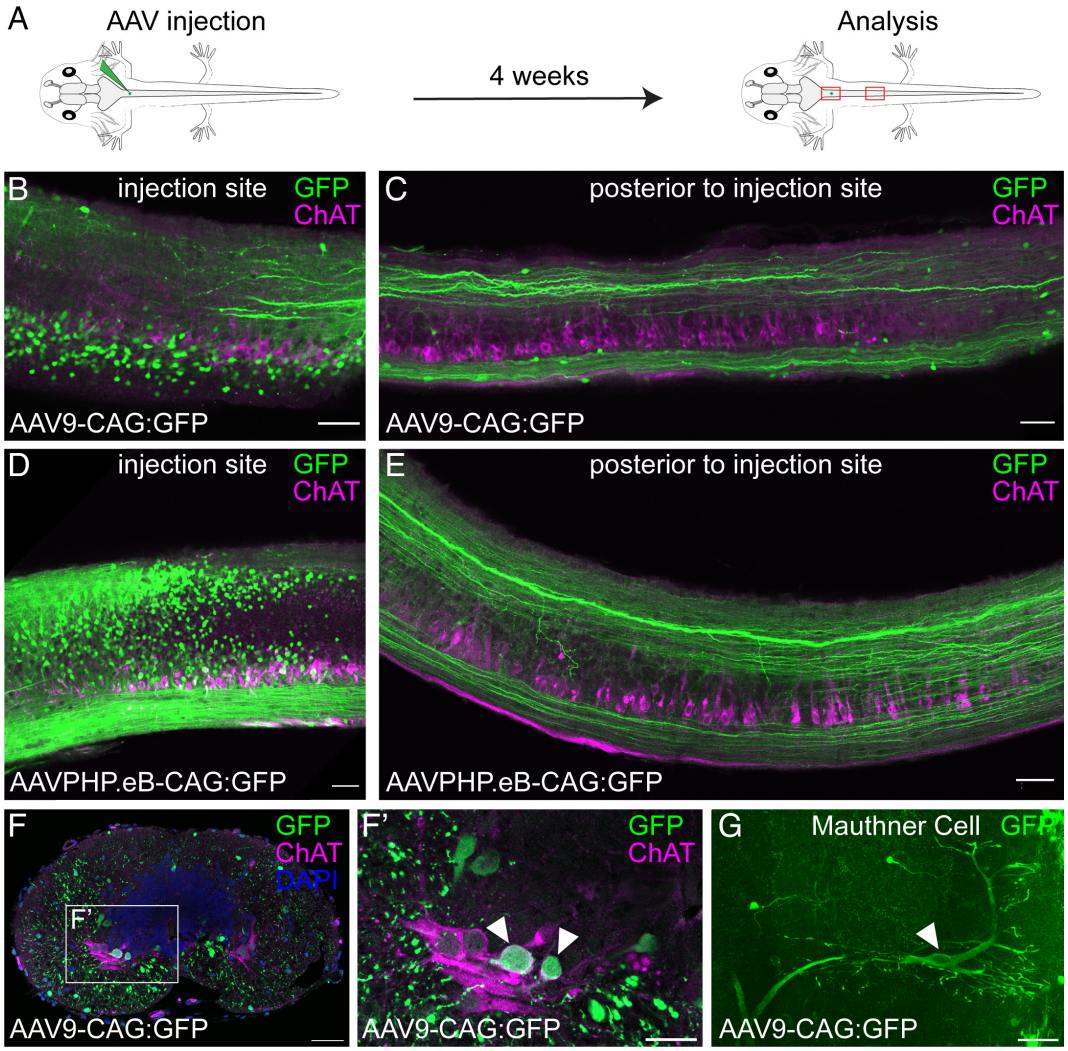

Fig. 3. AAV-mediated transduction of the axolotl spinal cord. (*A*) Schematic of injection region and the experimental paradigm. Each serotype was injected into the cervical spinal cord ventricle of larval axolotls (5 cm nose to tail) with FastGreen FCF added for visualization. Animals were housed at 22 degrees for 4 wk until the analysis. (*B*–*E*) Partial maximum projections of confocal images of wholemounts of spinal cords injected with either AAV9-CAG:GFP (*B* and *C*) or AAVPHP.eB-CAG:GFP (*D* and *E*) or respectively. Samples were labeled with anti-GFP (green) and anti-ChAT (magenta). All scale bars are 100 μm. (n = 4 axolotl injected for each serotype). (*F* and *F'*) Confocal image of cryosection of spinal cords injected with AAV9-CAG:GFP. Section was labeled with anti-GFP (green) and anti-ChAT (magenta) to identify motor neurons. Nuclei are counterstained with DAPI (blue). White arrowheads indicate coexpression of GFP and ChAT. [Scale bars, 100 μm (*E*) and 50 μm (*E'*).] (n = 4 axolotl injected). (*G*) Mauthner Cell (white arrowhead) labeled after injection with AAV9-CAG:GFP. (Scale bar is 100 μm.)

Dual-Vector Cotransduction Rates Following Coinjection of AAVs. The primary limitation of AAVs is their constrained packaging capacity, which is limited to approximately 4.7 kb (38). Exceeding this size threshold leads to a significant reduction in packaging efficiency (38). To address this constraint, a dual AAV vector system is often utilized to accommodate larger transgenes or to implement combinatorial systems such as Cre-loxP system (39). To assess the feasibility of cotransduction in the axolotl, we tested the following combination of dual AAV vectors: AAV8-CAG combined with AAV9-CAG:tdTomato (Fig. 5). We evaluated the extent of cotransduction, defined as the proportion of cells that were transduced by both vectors. Following the injection of AAV8-CAG:GFP and AAV9-CAG:tdTomato into the brain and spinal cord, we observed that AAV9-CAG:tdTomato generally transduced a higher number of cells in both the optic tectum and spinal cord (Fig. 5 *A*–*B*″). We quantified the percentage of AAV8-CAG:GFP cells that were also AAV9-CAG:tdTomato within defined volumes of the optic tectum and spinal cord, finding cotransduction rates ranging from 86 to 100% (Fig. 5 *C* and *D*). These results demonstrate that highly efficient AAV-mediated cotransduction is achievable in the axolotl nervous system using AAV8-CAG:GFP and AAV9-CAG:tdTomato.

Retrograde Transport Efficiency and Mapping of the Optic Tectum–Retina Axis. AAVs can be transported in different directions in neurons, which makes it possible to determine input and output of brain regions of interest. Different AAV serotypes can undergo both anterograde and retrograde transport; however, the natural ability for retrograde transport is rather low (40). Therefore, retrograde tracing-specific variants, such as AAVRG have been engineered (41). We sought to determine the transport direction of the different AAV serotypes. We decided to use the optic tectum and its anterograde input from the retina via the optic nerve (5) as an ideal test circuit. First, we assessed the ability and efficiency of retrograde transport. We injected AAV8-CAG:GFP, AAV9-CAG:GFP, and AAVRG-CAG:GFP into the right optic tectum hemisphere and harvested the left retina as well as the brain at 4 wk post injection (Fig. 6*A*). Using wholemount immunostaining of both tissues we aimed to determine the infection efficiency of the optic tectum as well as retrograde transport into the retina

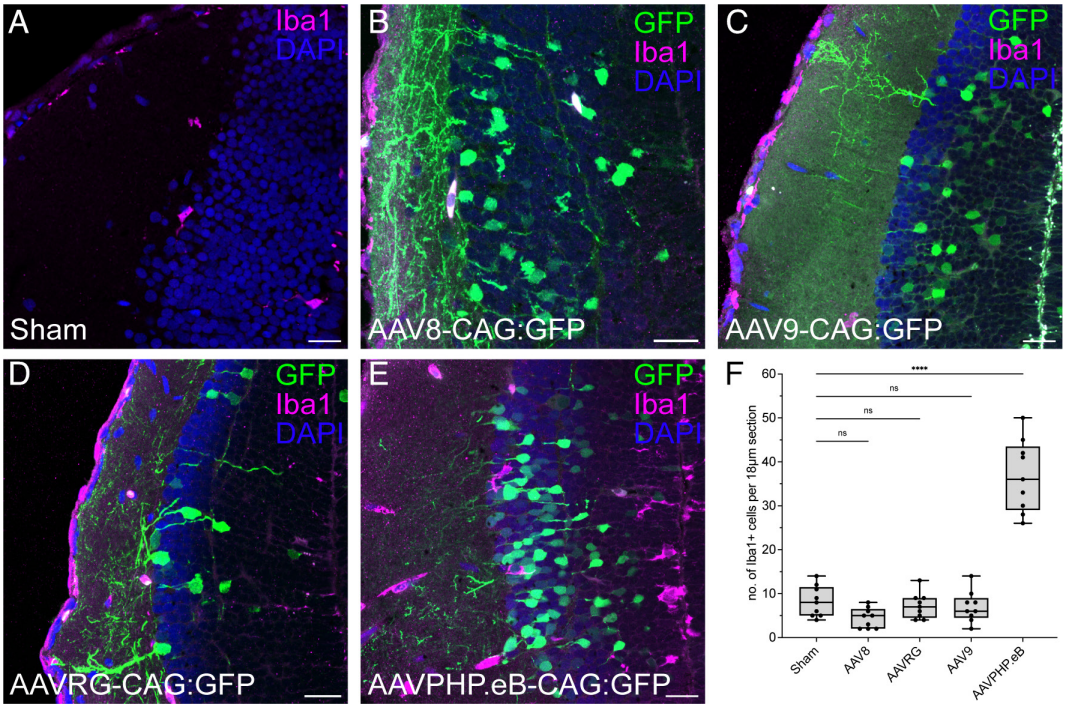

Fig. 4. Degree of AAV-induced immune cell infiltration varies based on serotype. (*A*) Confocal images of cryosections of sham brains. APBS was injected into the right optic tectum parenchyma of larval (3 cm nose to tail) animals which were housed at 22 degrees for 4 wk until the analysis. Sections were labeled with anti-Iba1 (magenta) to identify immune cells. Nuclei are counterstained with DAPI (blue). (*B–E*) Confocal images of cryosections of brains injected with either AAV8-CAG:GFP (*A*), AAV9-CAG:GFP (*B*), AAVRG-CAG:GFP (*C*), or AAVPHP.eB-CAG:GFP (*D*), respectively. Each serotype was injected into the right optic tectum parenchyma of larval (3 cm nose to tail) animals which were housed at 22 degrees for 4 wk until the analysis. Sections were labeled with anti-Iba1 (magenta) to identify immune cells. The fluorescent signal for GFP (green) was detected without antibody enhancement. Nuclei are counterstained with DAPI (blue). All scale bars are 50 µm. (*F*) Quantification of the number of Iba1-positive cells per section. Boxplot indicates "minimum," first quartile, median, third quartile, and "maximum." Statistical significance is calculated using one-way ANOVA followed by Tukey's multiple comparison. *P* values are Sham vs. AAVPHP.eB: **** < 0.0001, AAV8 vs. AAVPHP.eB ns = 0.4234, AAV9 vs. AAVPHP.eB: ns = 0.9797, AAVRG vs. AAVPHP.eB: ns = 0.9904. (n = 3 sections of three axolotls for each serotype or Sham).

(Fig. 6 *B–E*). While we found efficient infection of the optic tectum using all three serotypes (Fig. 6 *C–E*) the number of GFP-positive retinal ganglion cells was different for each serotype. We found that AAV8-CAG:GFP rarely labeled retinal ganglion cells (Fig. 6 *B* and *C*) but AAV9-CAG:GFP (Fig. 6 *B* and *D*) and AAVRG-CAG: GFP (Fig. 6 *B* and *E*) showed retrograde spreading properties. These results show that both AAV9-CAG:GFP and AAVRG-CAG:GFP can be retrogradely transported in neurons from the brain to the retina and that both serotypes can be used for assessing retrograde projections.

AAV-Mediated Transduction of the Axolotl Retina and Anterograde Transport. Next, we wanted to assess the ability of AAV serotypes to infect cells of the retina to ultimately determine anterograde spreading. It has been demonstrated previously that retinal tropism and transduction efficiency vary depending on the serotype and the route of delivery (42). We decided to inject AAVs intravitreally as this was the most feasible and reproducible method in small axolotl eyes. We injected AAV8-CAG:GFP, AAV9-CAG:GFP, and AAVRG-CAG:GFP into the vitreous of the right retina and waited for 4 wk to reach a high level of expression (Fig. 6*F*). We then fixed both retina and brain and analyzed for GFP expression focusing on which cell types of the retina had been infected and if optic nerves were labeled. We found that AAV8-CAG:GFP did not show any ability to transduce retinal cell types (Fig. 6 *G* and *J*). In contrast to that AAV9-CAG:GFP showed very efficient labeling of major retinal cell types, including retinal ganglion cells (Fig. 6 *H* and *J*). AAVRG-CAG:GFP showed labeling of retinal ganglion cells (Fig. 6*I*), however the efficiency was much lower compared to AAV9-CAG:GFP (Fig. 6*J*). When we analyzed the respective contralateral optic tectum hemisphere for labeling of projections from the optic nerve and found as expected no labeling in AAV8 transduced animals (Fig. 6*K*). In AAVRG-CAG:GFP injected animals we also did not detect any labeling of the optic nerve (Fig. 6*K*). In contrast all AAV9-CAG:GFP injected animals showed labeling of the optic nerve (Fig. 6 *K* and *L*). In addition to labeling retinal ganglion cells, we found that AAV9-CAG:GFP also labels other retinal cell types, including photoreceptors, amacrine cells, horizontal cells as well as retinal pigmented epithelial cells (Fig. 6*M*). Together, this shows that AAV9-CAG:GFP is efficient in transducing retinal cell types and can be used to trace retinal input into the brain. This also confirms the capability of AAV9-CAG:GFP to label cells across the axolotl central nervous system.

Tracing of the Retina-Brain Circuitry Using AAV9. After determining that AAV9-CAG:GFP showed high efficiency to infect retinal ganglion cells and anterograde spread in the optic nerve we decided to trace the retina brain circuitry in the axolotl using this serotype (Fig. 7 *A* and *B*). Optic nerve input into the brain has been determined in other salamander species by use of Golgi staining and horse radish peroxidase mediated tracing (5) and we thought this to be a suitable comparison to understand how well AAV9-CAG:GFP-mediated tracing could resolve those projections. In salamanders, fibers of the optic nerve have been found to distribute to five fields in the brain, the optic tectum, the pretectal nucleus, the area ventrolateralis pedunculi, the thalamus, and the hypothalamus (5). Using AAV9-CAG:GFP anterograde tracing we could detect fibers projecting into all these expected brain regions (Fig. 7 *C–H*). In addition, we also found GFP-labeled cell bodies in a region of the brain indicating that these neurons were retrogradely labeled (Fig. 7 *G* and *I*). Using the

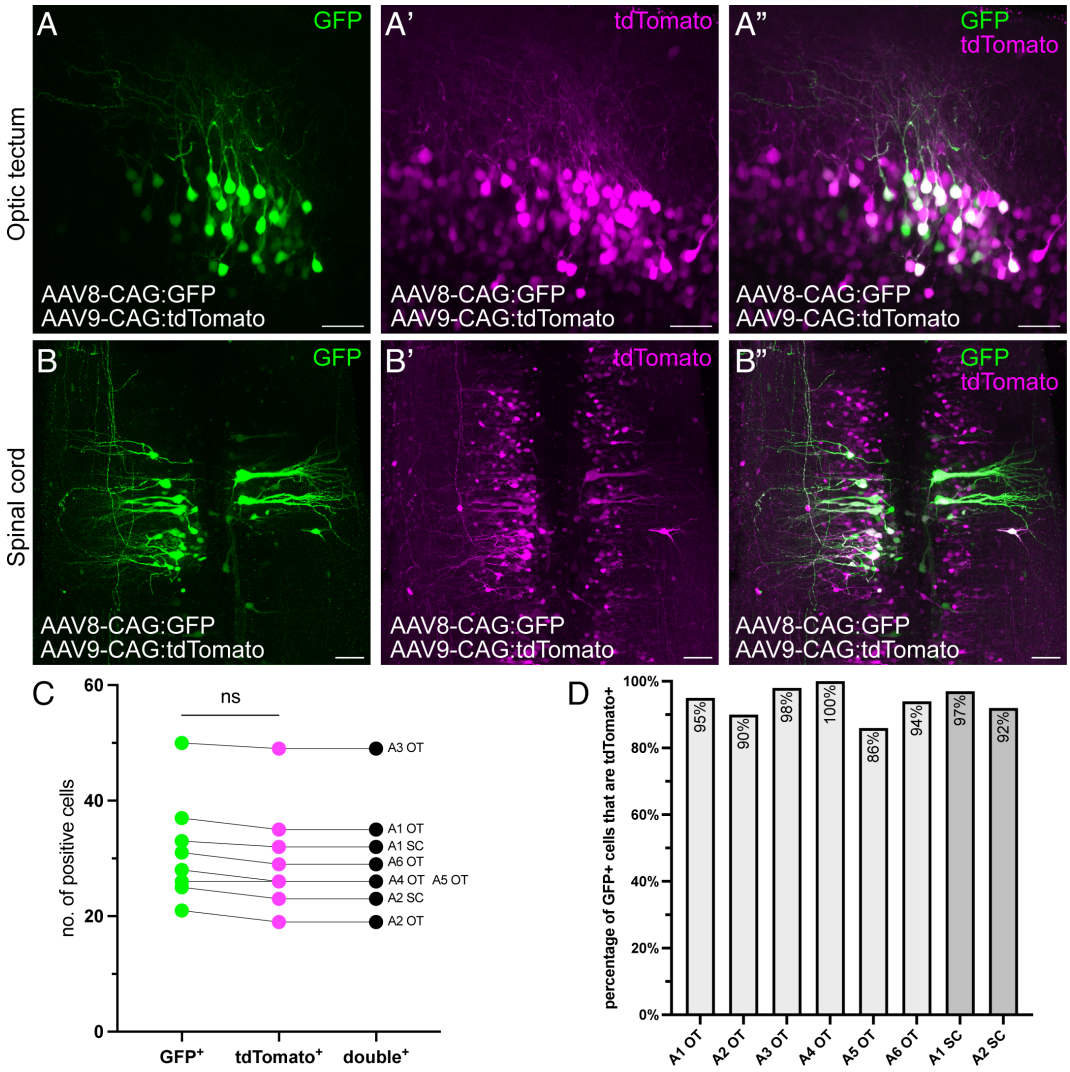

Fig. 5. Dual-vector cotransduction rates following coinjection of AAV8 and AAV9. (*A*) Partial maximum projections of confocal images of wholemounts of the optic tectum coinjected with AAV8-CAG:GFP (100 nL of a titer of 1.80E+13) and AAV9-CAG:tdTomato (100 nL of a titer of 2.50E+13) into the right parenchyma. All scale bars are 100 µm. (n = 6 axolotl). (*B*) Partial maximum projections of confocal images of wholemounts of spinal cords coinjected with AAV8-CAG:GFP (200 nL of a titer of 1.80E+13) and AAV9-CAG:tdTomato (200 nL of a titer of 2.50E+13). All scale bars are 100 µm. (n = 2 axolotl). (*C*) Quantification of the number of GFP-, tdTomato-, and double-positive cells per optic tectum or spinal cord volume. Statistical significance is calculated using the unpaired *t* test. *P* values are ns = 0.7469. (n = 6 axolotl for optic tectum and 2 axolotls for spinal cord. All AAV8-CAG:GFP-positive cells were counted, then it was determined how many of these are AAV9-CAG:tdTomato-positive.) (*D*) Quantification of the percentage of GFP-positive cells that are tdTomato positive per optic tectum or spinal cord volume.

sections and stainings for Pax6, we identified this region as the hypothalamus and the prethalamus (Fig. 7 *J* and *K*). As we had seen before that AAV9-CAG:GFP also shows the ability for retrograde spreading this result indicates that these neurons project into the retina. Various connections from the brain to the retina have been described as the retinopetal system in different vertebrates (43, 44). While retinopetal projections can arise from various brain regions, the origin in the hypothalamus is present in monkey (*Macaca nemestrina*) (45), cat (45), guinea pig (45), dog, (46) and teleost fish (47). Previously, in two salamander species (*Salamandra salamandra*, *Triturus vulgaris,* and *Triturus crestus*) retinopetal projections, originating in the pretectal area, have been found (48). In 1-y-old axolotls, Weber found nondegenerated fibers in the optic nerve several months after its section and located their cells of origin in the hypothalamus (49), consistent with our observations using AAV9-CAG:GFP-mediated tracing where we observed retinopetal projections originating from the hypothalamus but also the most ventral region of the prethalamus. When we revisited our AAVRG-CAG:GFP retina-brain tracing data we could detect cell bodies in the same brain regions (*SI Appendix,* Fig. S6 *A–C*). Thus, using AAV9-CAG:GFP we could faithfully trace all known input from the retina to the brain and additionally uncover the existence of retinopetal projections from the hypothalamus and prethalamus in the axolotl (Fig. 7*L*).

Discussion

In this study, we have investigated the functionality and efficiency of AAVs (AAV1, AAV2, AAV5, AAV8, AAV9, AAVRG, and AAVPHP.eB) to transduce cells in the axolotl brain, spinal cord, and retina. We found that except AAV2 all tested serotypes transduced cells of the axolotl brain, with AAV8, AAV9, and AAVPHP.eB being the most efficient viral vectors resulting in the most labeled cells per brain area. AAV8, AAV9, and AAVPHP.eB are also suited to transduce cells of the spinal cord, including motor neurons (AAV9 and AAVPHP.eB). However, AAVPHP.eB showed an increased immune cell infiltration of the injected brains even 1 mo after injection. Using the CAG promoter to drive expression of fluorescent proteins, we find that neurons rather than ependymoglia are preferentially labeled by AAV8, AAV9, and AAVPHP.

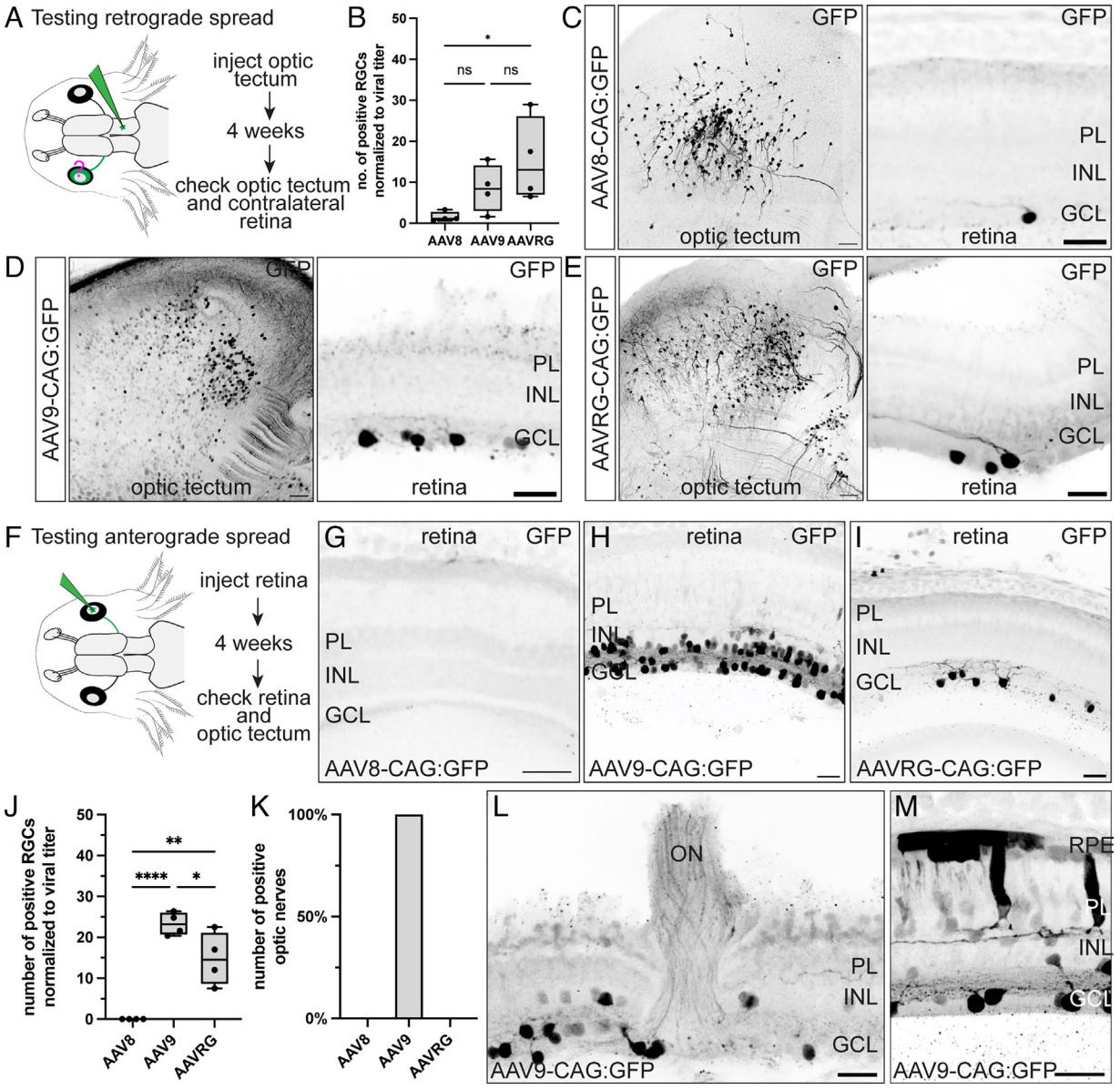

Fig. 6. Retrograde and anterograde spread properties of AAV8, AAV8, and AAVRG. (*A*) Schematic of experimental paradigm for testing AAV retrograde spread. AAV solution was injected into the right optic tectum parenchyma and the left (contralateral) retina was analyzed for the presence of cell bodies 4 wk later. (*B*) Quantification of GFP-positive cell bodies in the retinal ganglion cell layer of the whole retinal volume normalized to the viral titer. Boxplot indicates "minimum," first quartile, median, third quartile, and "maximum." Statistical significance is calculated using one-way ANOVA followed by Tukey's multiple comparison. *P* values are AAV8 vs. AAV9 ns = 0.3622, AAV8 vs. AAVRG * = 0.0449, AAV9 vs. AAVRG ns = 0.3714. (n = 4 axolotl for each serotype). (*C*–*E*) Optical sections from wholemount imaged retina and optic tectum of AAV8-CAG:GFP (*B*), AAV9-CAG:GFP (*C*), and AAVRG-CAG:GFP (*D*), respectively. Samples were labeled with anti-GFP (black, inverted image). Scale bars in optic tectum images are 100 μm. Scale bars in retina images are 50 μm. (*F*) Schematic of experimental paradigm for testing AAV anterograde spread. AAV solution was injected into the right retinal vitreous of larval (3 cm nose to tail) animals. Animals were housed at 22 degrees for 4 wk until the analysis. The left (contralateral) optic tectum hemisphere was analyzed for the presence of neuronal projections. (*G*–*I*) Optical sections from wholemount imaged retina and optic tectum of AAV8-CAG:GFP (*G*), AAV9-CAG:GFP (*H*), and AAVRG-CAG:GFP (*I*) respectively. Samples were labeled with anti-GFP (black, inverted image). All scale bars are 50 μm. (*J*) Quantification of GFP-positive retinal ganglion cells normalized to the viral titer (n = 4 axolotl for each serotype). Boxplot indicates "minimum," first quartile, median, third quartile, and "maximum." Statistical significance is calculated using one-way ANOVA followed by Tukey's multiple comparison. *P* values are AAV8 vs. AAV9 **** = <0.0001, AAV8 vs. AAVRG ** = 0.0016, AAV9 vs. AAVRG * = 0.374 (n = 3 sections each of 3 axolotls). (*K*) Quantification of GFP-positive cell projections in the optic tectum parenchyma shows that sAAV9 allow for efficient anterograde tracing while AAVRG is less efficient and AAV8 does not label any optic nerves. (n = 4 axolotl for each serotype). Boxplot indicates "minimum," first quartile, median, third quartile, and "maximum." (*L* and *M*) Optical sections from wholemount imaged retina transduced with AAV9-CAG:GFP. The sample was labeled with anti-GFP (black, inverted image). All scale bars are 50 μm. RGC-retinal ganglion cell, RPE-retinal pigmented epithelium, PL-photoreceptor layer, INL-inner nuclear layer, GCL-ganglion cell layer, ON-optic nerve.

eB. Finally, we demonstrate the use of AAV9 to label input and output projections of the retina through anterograde and retrograde tracing. This tracing approach led us to detect a cell population which projects from the brain to the retina.

We determined that in the axolotl AAV9 worked efficiently to transduce both brain and retinal neurons. Especially in the retina, AAV9 showed the highest potential when compared to AAV8 and AAVRG. Similarly to what has been observed in the mouse retina, we also found AAV9 to transduce retinal ganglion cells, amacrine cells, horizontal cells, and photoreceptors (50). AAV9 is of high interest because this serotype is widely used in rodents, especially because of its capacity to cross the blood–brain barrier (51). Furthermore, AAV9 is one of the few serotypes described to have anterograde transsynaptic spreading ability when used to express Cre recombinase and injected into loxP reporter mice (52). We have not tested these two abilities of AAV9 in the axolotl yet;

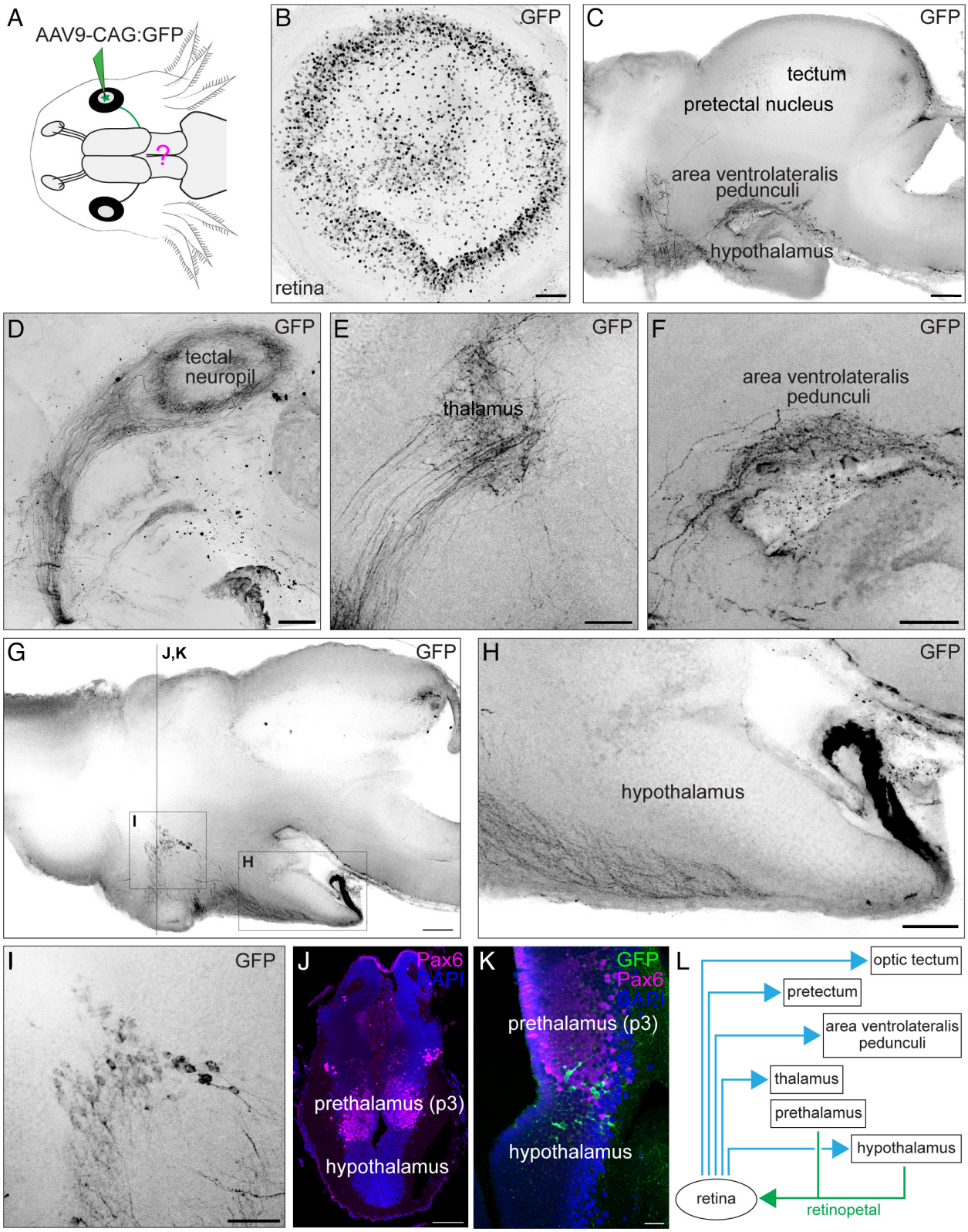

Fig. 7. Tracing the retina-brain circuit using AAV9-CAG. (*A*) Schematic of experimental paradigm. The right retinal vitreous of larval (3 cm nose to tail) animals was injected with AAV9-CAG:GFP. Animals were housed at 22 degrees for 4 wk until the analysis. (*B*) Wholemount maximum intensity projection of the retina transduced with AAV9-CAG:GFP. The sample was labeled with anti-GFP (black, inverted image). (Scale bar is 200 μm.) (*C*) Wholemount maximum intensity projection of the brain after retinal transduction with AAV9-CAG. The sample was labeled with anti-GFP (black, inverted image). (Scale bar is 200 μm.) (*D–H*) Wholemount maximum intensity projection of brain regions with neuronal projection from retina after retinal transduction with AAV9-CAG. The sample was labeled with anti-GFP (black, inverted image). Scale bar in D is 200 μm. All other scale bars are 100 μm. (*I*) Wholemount maximum intensity projection of the anterior hypothalamus region with retrogradely labeled cells. The sample was labeled with anti-GFP (black, inverted image). (Scale bar is 100 μm.) (*J*) Sectioning plane of the diencephalon with the prethalamus (p3) marked by Pax6 (magenta) and the anterior hypothalamus region below. (Scale bar is 200 μm.) (*K*) Section of the diencephalon with the prethalamus (p3) and the anterior hypothalamus region with retrogradely labeled cells (green). The sample was labeled with anti-GFP (green), Pax6 (magenta) to label the prethalamus and DAPI (blue). (Scale bar is 50 μm.) (n = 8 axolotl). (*L*) Projections of the retina and different brain regions revealed by tracing with AAV9-CAG:GFP.

however, the high efficiency of AAV9 as well as the availability of loxP reporter animals will make this possible in the future.

AAV9 injection in the axolotl retina has allowed us to map the circuitry between the retina and the brain and we could recover all known projections of the optic nerve. Additionally, due to the retrograde spreading abilities of AAV9 we found the existence of retinopetal cells in the hypothalamus and prethalamus of the axolotl. In general, projections from the brain to the retina have been found in a variety of vertebrates, ranging from lampreys (53), teleost fish (47), salamanders (48), reptiles (43), birds (54) to mammals (44). Specifically, projections from the hypothalamus to the retina have been found in mammals (45), amphibians (49), and fish (47). The retinopetal system represents a feedback mechanism that allows the brain to influence and fine-tune retinal activity (55). Although its exact roles are not fully elucidated, its importance in modulating visual processing, attention, and circadian rhythms is becoming increasingly recognized (56). Whether this function is conserved in the axolotl will be of future interest. While retinopetal projection patterns to the inner nuclear layer have been mapped in the retina of other species (57), future investigation of this cell population in the axolotl will reveal the conservation of target regions of such projections.

Here, we have used AAVs to express fluorescent proteins in the axolotl brain, the spinal cord, and the retina. In other species, AAVs are used for transducing neurons with functional reporter constructs, such as GCaMP-based calcium reporters which enable in vivo imaging of neuronal activity (58). Given the continuous evolution of such reporters and the ongoing advancements tool development in neuroscience, AAVs offer the possibility to stay up to date with future sensor developments. Their use in the axolotl is particularly advantageous as they circumvent the need for generating transgenic lines. The introduction of AAV-based neuronal labeling into the axolotl nervous system opens possibilities for future applications, including mapping circuit reestablishment after injury and regeneration. Since AAVs are transient vectors, we assessed the long-term stability of expression by transducing with AAV9-CAG:tdTomato and found that expression remains stable for up to 2 mo (*SI Appendix,* Fig. S7). This supports the potential use of AAVs in regeneration studies, as demonstrated in our previous experiments (3).

Additionally, the potential for transsynaptic labeling, either through transsynaptic AAVs (52) or by combining AAVs with rabies virus-based monosynaptic retrograde mapping (59), holds promise for probing circuit establishment and reestablishment in the axolotl with unprecedented resolution. Notably, rabies virus-mediated transsynaptic tracing has recently been successfully implemented in zebrafish (60). Furthermore, recent advancements, such as AAV-based screens, for example AAV perturb-seq in the mouse brain (60, 61), could potentially be adapted to the axolotl to perform in vivo screens. Taken together, AAVs as gene transfer tools will allow for various experimental opportunities that were previously unapproachable in the axolotl and will likely transform the study of nervous system regeneration.

Materials and Methods

Materials. All materials used in this study are listed in *SI Appendix,* Table S1.

Axolotl. White (d/d) axolotls were used for all experiments. All animals were bred and maintained in IMP facilities and each animal is kept individually. All handling and surgical procedures were carried out in accordance with the local ethics committee guidelines. Animal experiments were performed as approved by the Magistrate of Vienna (Genetically 10 Modified Organism Office and MA58, City of Vienna, Austria, license GZ51072/2019/16 and license GZ665226/2019/21). Axolotl husbandry was performed as described previously. Animals of a size of 3 cm, 5 cm, or 10 cm nose to tail were used for all experiments. We were blinded to the sex of the animals as they were not genotyped and sexual characteristics are apparent at the stages we explored.

Method Details

Injection of AAVs into the Brain. AAVs were purchased from Addgene and injected at the maximum concentration (titer ≥ 7×10^{12} vg/mL; for detailed viral titers, see *SI Appendix,* Tables S2 and S3). FastGreen FCF was added for visualization. Before injection, axolotls were fully anesthetized in 0.03% benzocaine. In small (3 cm long) animals the skin and skull are still soft and can be pierced with 27G needle to generate an opening for the injection needle. In big (10 cm long) animals the skin was removed using scissors and forceps and a small incision into the skull was made using a 27G needle. Micropipettes pulled from borosilicate glass were filled with the virus solution and used for pressure injection into the desired region of the brain. In 3 cm animals roughly 0.1 µL virus solution per animal and in 10 cm animals 0.5 µL virus solution per animal were injected. After surgery, animals were kept in standard holding tanks and the brains were harvested at 4 wk after injection. Sham animals were injected with APBS (amphibian PBS, 70% 1 × PBS) with FastGreen FCF into the right optic tectum parenchyma of larval animals (3 cm long). For more details, see *SI Appendix,* Table S3. When injecting the optic tectum parenchyma unilaterally in 3 cm animals we noted that in some serotypes (especially AVV8, AAV9, and AAVPHP.eB) bilateral hemisphere labeling could be detected, which could be due to some viral solution leaking into the ventricle. For more details, see *SI Appendix,* Table S4.

Injection of AAVs into the Retina. To inject into the retina, a small incision was made in the cornea next to the lens with a microknife and the borosilicate glass injection needle was inserted into the vitreous. The approximate volume of the vitreous was calculated from measurements with digital calipers as described previously (62). The vitreous cavity was approximated as the difference between the volume of the entire eyeball minus the volume of the lens. According to this calculation, 0.1 µL of virus solution per animal is injected in 3 cm long animals. After 4 wk the retinae and brains were harvested. For more details, see *SI Appendix,* Table S3.

Injection of AAVs into the Spinal Cord. AAVs were mixed with FastGreen FCF for visualization. Before injection, axolotls were fully anesthetized in 0.03% benzocaine. Micropipettes pulled from borosilicate glass were filled with the virus solution and used for pressure injection into the desired region. The needle was inserted into the spinal cord canal through the dorsal trunk muscle. In 5 cm animals, roughly 0.2 µL virus solution per animal were injected. After surgery, animals were kept in standard holding tanks and the brains were harvested at 4 wk after injection. For more details, see *SI Appendix,* Table S3.

Brain, Eye, and Spinal Cord Collection for HCR or Immunofluorescence. For tissue harvesting, axolotls were fully anesthetized, decapitated with scissors, and brains, eyes, or spinal cords were extracted and fixed overnight in 4% paraformaldehyde at 4 °C on a horizontal shaker. Fixed samples were washed six times for 30 min each with 1 × PBS on a horizontal shaker at 4 °C. For further use, samples were either incubated overnight in 30% sucrose in 1 × PBS at 4 °C if used for cryosectioning or used immediately for wholemount immunofluorescence. For long-term storage, samples were dehydrated in a methanol/1 × PBS series (25%, 50%, 75%, two times 100% for 30 min each at 4 °C on a horizontal shaker) and stored in 100% Methanol at −20 °C.

Cryosections. Cryosections were generated as described previously (3).

HCR Probe Design and HCR on Cryosections. HCR probe pairs were designed as previously published (3). Detailed probe sequences have been published previously (3) except for the AAV probe for which the sequence is listed in *SI Appendix*, Table S5. HCR was performed as previously published (3).

Immunofluorescence on Cryosections. Immunofluorescence on cryosections was performed as described previously (3). Primary antibody dilutions are Rabbit anti-RFP (1:500 in 1 × PBST), Rabbit anti-GFP (1:500 in 1 × PBST), Mouse anti-GFP (1:500 in 1 × PBST), Mouse anti-GFAP-Cy3 Conjugated, Clone G-A-5 (1:500 in 1 × PBST), Rabbit anti-Iba1 (1:500 in 1 × PBST), Goat anti-ChAT (1:200 in 1 × PBST), Mouse anti-Pax6 (1:200 in 1 × PBST). In general, amplification of the AAV-mediated signals (GFP or Cherry in this case) by immunofluorescence is preferable, as endogenous signal can be variable between cells.

CUBIC Clearing and Wholemount Immunostaining of AAV-Injected Brains, Retinae, and Spinal Cords. Clearing and staining was performed using CUBIC as described previously (3, 63). Primary antibody dilutions are Rabbit anti-RFP (1:500 in 1 × PBST), Rabbit anti-GFP (1:500 in 1 × PBST), Mouse anti-GFP (1:500 in 1 × PBST), Mouse anti-GFAP-Cy3 Conjugated, Clone G-A-5 (1:500 in 1 × PBST), Rabbit anti-Iba1 (1:500 in 1 × PBST), Goat anti-ChAT (1:500 in 1 × PBST), Mouse anti-Pax6 (1:200 in 1 × PBST).

Microscopy. Cleared samples were imaged in Ibidi glass bottom dishes on an inverted Zeiss LSM980 Axio Observer (inverted) confocal microscope (10×/0.3 EC plan-neofluar objective). Cryosections were using a 20×/0.8 plan-apochromat objective. Image acquisition and automatic stitching was performed using ZenBlue 3.2. Images were prepared using FIJI (based on ImageJ1.53c). Inverted images in Figs. 6 and 7, and *SI Appendix*, Fig. S6 were produced using the Invert LUT function in FIJI.

Quantification and Statistical Analysis

Somata and Nuclei Counting. Cell somata counts were performed using the FIJI cell counterplugin. Regions and sections for analysis were selected in a way that they represent the same anatomical location, and we performed soma counts in standardized volumes of 200 × 200 × 80 μm^3 (in 3 cm animals) and 200 × 200 × 40 μm^3 (in 10 cm animals) to accommodate for slight variations. We always chose the injected region (either optic tectum in 3 cm or dorsal telencephalon in 10 cm animals) to count transduced cells. Nuclei on cryosections were counted using Cellpose 2.0 using the CPx model. Each segmentation was inspected and manually corrected if needed. To allow for better comparison, each viral serotype was normalized by its respective titer.

Statistical Analysis. Unpaired *t* tests and one-way ANOVA were carried out using Prism version 10 (GraphPad; San Diego, CA); $P < 0.05$ was considered statistically significant.

Data, Materials, and Software Availability. All study data are included in the article and/or *SI Appendix*.

ACKNOWLEDGMENTS. We would like to thank the members of the Tanaka lab for discussions, input, and support. We thank the BioOptics facility IMP/IMBA Core Facilities for outstanding service and the animal care team for excellent axolotl care. K.L. was supported by a Long-Term Fellowship from the Human Frontier Science Program (LT000605/2018-L) and a Marie Sklodowska-Curie fellowship (101033093), E.M.T. was supported by the Special research programme of the Austrian Science Fund (Project F78) and an Advanced Grant of the European Research Council (RegGeneMems, 742046). For the purpose of Open Access, the authors have applied a CC BY public copyright license to any Author Accepted Manuscript (AAM) version arising from this submission.

1. M. Okamoto, H. Ohsawa, T. Hayashi, K. Owaribe, P. A. Tsonis, Regeneration of retinotectal projections after optic tectum removal in adult newts. *Mol. Vis.* **13**, 2112–2118 (2007).
2. R. Amamoto *et al.*, Adult axolotls can regenerate original neuronal diversity in response to brain injury. *Elife* **5**, e13998 (2016).
3. K. Lust *et al.*, Single-cell analyses of axolotl telencephalon organization, neurogenesis, and regeneration. *Science* **377**, eabp9262 (2022).
4. T. Finkenstädt, S. O. Ebbesson, J. P. Ewert, Projections to the midbrain tectum in Salamandra salamandra L. *Cell Tissue Res.* **234**, 39–55 (1983).
5. C. Judson Herrick, *The Brain of the Tiger Salamander: Ambystoma Tigrinum* (The University of Chicago Press, Chicago, 1948).
6. J. Woych *et al.*, Cell-type profiling in salamanders identifies innovations in vertebrate forebrain evolution. *Science* **377**, eabp9186 (2022).
7. S. Khattak, E. M. Tanaka, Transgenesis in axolotl (Ambystoma mexicanum). *Methods Mol. Biol.* **1290**, 269–277 (2015).
8. A. Rodrigo Albors, E. M. Tanaka, High-efficiency electroporation of the spinal cord in larval axolotl. *Methods Mol. Biol.* **1290**, 115–125 (2015).
9. C. R. Oliveira *et al.*, Pseudotyped baculovirus is an effective gene expression tool for studying molecular function during axolotl limb regeneration. *Dev. Biol.* **433**, 262–275 (2018).
10. T.-H. Kuo, J. L. Whited, Pseudotyped retroviruses for infecting axolotl. *Methods Mol. Biol.* **1290**, 127–140 (2015).
11. S. Roy, D. M. Gardiner, S. V. Bryant, Vaccinia as a tool for functional analysis in regenerating limbs: Ectopic expression of Shh. *Dev. Biol.* **218**, 199–205 (2000).
12. S. Khattak *et al.*, Foamy virus for efficient gene transfer in regeneration studies. *BMC Dev. Biol.* **13**, 17 (2013).
13. D. L. Haggerty, G. G. Grecco, K. C. Reeves, B. Atwood, Adeno-associated viral vectors in neuroscience research. *Mol. Ther. Methods Clin. Dev.* **17**, 69–82 (2020).
14. L. C. Parr-Brownlie *et al.*, Lentiviral vectors as tools to understand central nervous system biology in mammalian model organisms. *Front. Mol. Neurosci.* **8**, 14 (2015).
15. J.-H. Wang, D. J. Gessler, W. Zhan, T. L. Gallagher, G. Gao, Adeno-associated virus as a delivery vector for gene therapy of human diseases. *Signal Transduct. Target. Ther.* **9**, 1–33 (2024).
16. A. Bennett, M. Mietzsch, M. Agbandje-McKenna, Understanding capsid assembly and genome packaging for adeno-associated viruses. *Future Virol.* **12**, 283–297 (2017).
17. S. S. Issa, A. A. Shaimardanova, V. V. Solovyeva, A. A. Rizvanov, Various AAV serotypes and their applications in gene therapy: An overview. *Cells* **12**, 785 (2023).
18. K. Y. Chan *et al.*, Engineered AAVs for efficient noninvasive gene delivery to the central and peripheral nervous systems. *Nat. Neurosci.* **20**, 1172–1179 (2017).
19. N. L. Benavidez *et al.*, Organization of the inputs and outputs of the mouse superior colliculus. *Nat. Commun.* **12**, 4004 (2021).
20. R. C. Challis *et al.*, Adeno-associated virus toolkit to target diverse brain cells. *Annu. Rev. Neurosci.* **45**, 447–469 (2022).
21. D. Goertsen *et al.*, AAV capsid variants with brain-wide transgene expression and decreased liver targeting after intravenous delivery in mouse and marmoset. *Nat. Neurosci.* **25**, 106–115 (2022).
22. N. Rook *et al.*, AAV1 is the optimal viral vector for optogenetic experiments in pigeons (Columba livia). *Commun. Biol.* **4**, 100 (2021).
23. D. N. Düring *et al.*, Fast retrograde access to projection neuron circuits underlying vocal learning in songbirds. *Cell Rep.* **33**, 108364 (2020).
24. E. Hisey, M. G. Kearney, R. Mooney, A common neural circuit mechanism for internally guided and externally reinforced forms of motor learning. *Nat. Neurosci.* **21**, 589–597 (2018).
25. H. Norimoto *et al.*, A claustrum in reptiles and its role in slow-wave sleep. *Nature* **578**, 413–419 (2020).
26. E. C. B. Jaeger *et al.*, Adeno-associated viral tools to trace neural development and connectivity across amphibians. *Dev Cell* (2024). https://doi.org/10.1016/j.devcel.2024.10.025.
27. P. Zhu *et al.*, Optogenetic dissection of neuronal circuits in zebrafish using viral gene transfer and the Tet system. *Front. Neural Circuits* **3**, 21 (2009).
28. J. L. Whited, J. A. Lehoczky, C. J. Tabin, Inducible genetic system for the axolotl. *Proc. Natl. Acad. Sci. U.S.A.* **109**, 13662–13667 (2012).
29. H. M. T. Choi *et al.*, Third-generation hybridization chain reaction: Multiplexed, quantitative, sensitive, versatile, robust. *Development* **145**, dev165753 (2018).
30. M. Maden, L. A. Manwell, B. K. Ormerod, Proliferation zones in the axolotl brain and regeneration of the telencephalon. *Neural Dev.* **8**, 1 (2013).
31. J. M. Veres, T. Andrasi, P. Nagy-Pal, N. Hajos, CaMKIIα promoter-controlled circuit manipulations target both pyramidal cells and inhibitory interneurons in cortical networks. *eNeuro* **10**, ENEURO.0070-23.2023 (2023).
32. L. McHedlishvili, H. H. Epperlein, A. Telzerow, E. M. Tanaka, A clonal analysis of neural progenitors during axolotl spinal cord regeneration reveals evidence for both spatially restricted and multipotent progenitors. *Development* **134**, 2083–2093 (2007).
33. L. A. Wiley *et al.*, The degree of adeno-associated virus-induced retinal inflammation varies based on serotype and route of delivery: Intravitreal, subretinal, or suprachoroidal. *Hum. Gene Ther.* **34**, 530–540 (2023).
34. Y. Guo *et al.*, High-titer AAV disrupts cerebrovascular integrity and induces lymphocyte infiltration in adult mouse brain. *Mol. Ther. Methods Clin. Dev.* **31**, 101102 (2023).

35. D. Ito *et al.*, Microglia-specific localisation of a novel calcium binding protein, Iba1. *Brain Res. Mol. Brain Res.* **57**, 1–9 (1998).
36. L. F. Eng, R. S. Ghirnikar, GFAP and astrogliosis. *Brain Pathol.* **4**, 229–237 (1994).
37. V. Kroehne, D. Freudenreich, S. Hans, J. Kaslin, M. Brand, Regeneration of the adult zebrafish brain from neurogenic radial glia-type progenitors. *Development* **138**, 4831–4840 (2011).
38. Z. Wu, H. Yang, P. Colosi, Effect of genome size on AAV vector packaging. *Mol. Ther.* **18**, 80–86 (2010).
39. P. Datta *et al.*, Delivering large genes using adeno-associated virus and the CRE-lox DNA recombination system. *Hum. Mol. Genet.* **33**, 2094–2110 (2024).
40. M. M. Surdyka, M. Figiel, Retrograde capabilities of adeno-associated virus vectors in the central nervous system. *BioTechnologia (Pozn)* **102**, 473–478 (2021).
41. D. G. R. Tervo *et al.*, A designer AAV variant permits efficient retrograde access to projection neurons. *Neuron* **92**, 372–382 (2016).
42. I. C. Han *et al.*, Retinal tropism and transduction of adeno-associated virus varies by serotype and route of delivery (intravitreal, subretinal, or suprachoroidal) in rats. *Hum. Gene Ther.* **31**, 1288–1299 (2020).
43. H. Schnyder, H. Künzle, The retinopetal system in the turtle Pseudemys scripta elegans. *Cell Tissue Res.* **234**, 219–224 (1983).
44. J. Repérant, S. Araneda, D. Miceli, M. Medina, J. P. Rio, Serotonergic retinopetal projections from the dorsal raphe nucleus in the mouse demonstrated by combined [(3)H] 5-HT retrograde tracing and immunolabeling of endogenous 5-HT. *Brain Res.* **878**, 213–217 (2000).
45. J. L. Labandeira-Garcia, M. J. Guerra-Seijas, F. Gonzalez, R. Perez, C. Acuña, Location of neurons projecting to the retina in mammals. *Neurosci. Res.* **8**, 291–302 (1990).
46. H. Terubayashi, H. Fujisawa, M. Itoi, Y. Ibata, Hypothalamo-retinal centrifugal projection in the dog. *Neurosci. Lett.* **40**, 1–6 (1983).
47. P. D. Prasada Rao, A. P. Kulkarni, Retinopetal neuronal system in the brain of an air-breathing teleost fish, Channa punctata. *Cell Tissue Res.* **263**, 385–394 (1991).
48. B. Fritzsch, W. Himstedt, Pretectal neurons project to the salamander retina. *Neurosci. Lett.* **24**, 13–17 (1981).
49. A. Weber, Centrifugal fibers in the optic nerve of the Axolotl. *Bull. Histol. Appl. Physiol. Pathol. Tech. Microsc.* **22**, 39 (1945).
50. B. Lei, K. Zhang, Y. Yue, A. Ghosh, D. Duan, Adeno-associated virus serotype-9 mediated retinal outer plexiform layer transduction is mainly through the photoreceptors. *Adv. Exp. Med. Biol.* **664**, 671–678 (2010).
51. K. D. Foust *et al.*, Intravascular AAV9 preferentially targets neonatal neurons and adult astrocytes. *Nat. Biotechnol.* **27**, 59–65 (2009).
52. B. Zingg *et al.*, AAV-mediated anterograde transsynaptic tagging: Mapping corticocollicular input-defined neural pathways for defense behaviors. *Neuron* **93**, 33–47 (2017).
53. N. P. Vesselkin, J. P. Rio, J. Repérant, N. B. Kenigfest, V. O. Adanina, Retinopetal projections in lampreys. *Brain Behav. Evol.* **48**, 277–286 (1996).
54. H. Uchiyama *et al.*, Attentional signals projecting centrifugally to the avian retina: A dual contribution to visual search. *Vision Res.* **195**, 108016 (2022).
55. R. A. Warwick *et al.*, Top-down modulation of the retinal code via histaminergic neurons of the hypothalamus. *Sci. Adv.* **10**, eadk4062 (2024).
56. V. Vereczki, K. Köves, Á. Csáki, Current state of knowledge on the centrifugal visual system (including the pinealo-to-retinal connection) in mammals and its hypothesized role in circadian rhythms. *Open Explor.* **3**, 51–64 (2019).
57. M. J. Gastinger, N. Tian, T. Horvath, D. W. Marshak, Retinopetal axons in mammals: Emphasis on histamine and serotonin. *Curr. Eye Res.* **31**, 655–667 (2006).
58. S. Grødem *et al.*, An updated suite of viral vectors for in vivo calcium imaging using intracerebral and retro-orbital injections in male mice. *Nat. Commun.* **14**, 608 (2023).
59. E. J. Kim, M. W. Jacobs, T. Ito-Cole, E. M. Callaway, Improved monosynaptic neural circuit tracing using engineered rabies virus glycoproteins. *Cell Rep.* **15**, 692–699 (2016).
60. C. Satou *et al.*, A viral toolbox for conditional and transneuronal gene expression in zebrafish. *Elife* **11**, e77153 (2022).
61. A. J. Santinha *et al.*, Transcriptional linkage analysis with in vivo AAV-Perturb-seq. *Nature* **622**, 367–375 (2023).
62. P. A. Raymond, M. J. Reifler, P. K. Rivlin, Regeneration of goldfish retina: Rod precursors are a likely source of regenerated cells. *J. Neurobiol.* **19**, 431–463 (1988).
63. K. Matsumoto *et al.*, Advanced CUBIC tissue clearing for whole-organ cell profiling. *Nat. Protoc.* **14**, 3506–3537 (2019).